Contents lists available at ScienceDirect

Brain Behavior and Immunity

journal homepage: http://ees.elsevier.com

Novel phloroglucinol derivative Compound 21 protects experimental autoimmune encephalomyelitis rats via inhibiting Th1/Th17 cell infiltration

Zhe Zhao, Xiu-qi Bao, Zihong Zhang, Fangyuan Li, Hui Liu, Dan Zhang*

State Key Laboratory of Bioactive Substrate and Function of Natural Medicine, Institute of Materia Medica, Chinese Academy of Medical Sciences and Peking Union Medical College, 1 Xian Nong Tan Street, Beijing 100050, China

ARTICLE INFO

Keywords
Multiple sclerosis
Experimental autoimmune encephalomyelitis
Th1 cell
Th17 cell
Inflammation

ABSTRACT

Multiple sclerosis (MS) is a chronic autoimmune disease characterized by inflammatory infiltration and demyelination in the central nervous system (CNS). Among the factors involved in the immunological mechanisms of MS, T helper 1 (Th1) cells and T helper 17 (Th17) cells play a critical role. Compound 21, a novel phloroglucinol derivative, significantly protected myelin from damage in our previous study. However, it remains unclear whether this compound affects MS. In this study, the experimental autoimmune encephalomyelitis (EAE) rat model was established to mimic the pathological process of MS and evaluate the neuroprotective effect of Compound 21. The results illustrated that Compound 21 treatment notably attenuates neurological deficits, immune infiltration, and demyelination in EAE rats. Our mechanistic investigation revealed that Compound 21 treatment reduces the population of Th1/Th17 cells and inhibits their infiltration into the CNS. Furthermore, we found that the inhibition of Th1/Th17 cell infiltration is related to the direct suppression of Th1/Th17 cell differentiation and the inhibition of proinflammatory microglial cells. Collectively, these results confirm that Compound 21 suppresses infiltrated Th1/Th17 cells to alleviate demyelination in EAE rats, suggesting its potential role as a novel candidate for MS treatment.

1. Introduction

Multiple sclerosis (MS) is a chronic demyelinating disease of the central nervous system (CNS) with a wide range of symptoms such as difficulty walking, fatigue, pain, and memory loss [1]. The primary pathological features of MS are inflammatory infiltration in the white matter and demyelination of the CNS. The pathogenesis of MS is related to genetics [2,3], environment [4–6], and immunology [7]. Although the specific mechanisms of MS are still unclear, both innate and adaptive immune systems have been shown to be important in the development of this demyelinating disease. Recruited by specific autoimmune antigens, T cells invade into the CNS and progressively damage myelin sheaths. This damage leads to further inflammatory processes, which induce the activation of other immune cells and the release of inflammatory cytokines. All these factors work together to enhance the loss of myelin and eventually lead to permanent damage of the nerves [8,9]. To investigate the mechanisms of MS, various animal models have been developed. The experimental autoimmune encephalomyelitis (EAE) model, an animal model that is developed by immunization with myelin basic protein (MBP), has many neuropathological characteristics in common with MS. This model is widely used to investigate the mechanisms of MS and develop potential candidates for MS treatment [10,11].

Many therapeutic agents that are currently available to treat MS focus on the overactivated immune response [12]. These drugs can be divided into two categories. The first category broadly inhibits the immune response and includes interferon (IFN)-β [13], glucocorticoids [14], and cyclosporin A [15]. The second category targets specific receptors of immune cells and includes fingolimod (FTY720)Calabresi et al., 2014; Chitnis et al., 2018; DiMarco et al., 2014; Lublin et al., 2016[16–19], natalizumab [20], and alemtuzumab [21]. Although these drugs can effectively relieve the symptoms of MS and reduce the frequencies of relapse, most have shown severe adverse effects including sudden fever, headache, or serious infections caused by the disturbed immune system. Therefore, the development of novel drugs with new targets is urgently needed to improve treatment for patients with MS.

To aid in this development, many scientists have been exploring the underlying pathogenesis of MS. Several immunological studies have demonstrated the important role of the overacti-

* Corresponding author.
E-mail address: danzhang@imm.ac.cn (D. Zhang)

https://doi.org/10.1016/j.bbi.2020.03.009
Received 13 November 2019; Received in revised form 9 March 2020; Accepted 11 March 2020
Available online xxx
0889-1591/

vated immune response [2,7]. Although the immune mechanisms are complicated, two primary pathogenic subgroups of $CD4^+$ T cells—T helper 17 (Th17) and T helper 1 (Th1)—are thought to play a critical role in MS [22–25]. Both cell types can invade the CNS through the blood–brain barrier with the assistance of cytokines they secrete, then promote neuroinflammation and myelin sheath damage [26,27]. After the activation and invasion of Th1/Th17 cells into the CNS, the proinflammatory microenvironment of CNS is important for the maintenance of Th1/Th17 activation in the CNS. The proinflammatory microglial cells in the CNS can produce inflammatory cytokines including IFN-γ, interleukin (IL) 12, and IL-23 to stabilize the infiltrated Th1/Th17 cell activation [28,29]. Collectively, agents targeting the suppression of Th1/Th17 infiltration are a potential approach to treat MS.

Our previous studies have demonstrated that a novel phloroglucinol derivative, Compound 21, effectively suppresses neuroinflammation both *in vivo* and *in vitro* [30,31]. In addition, our recent investigation showed that Compound 21 remarkably attenuates demyelination in mice intoxicated by cuprizone (CPZ)[32]. However, it remains unclear whether the compound is protective against MS. The present study aimed to evaluate the effect of Compound 21 in the EAE rat model and further explore the underlying mechanisms.

2. Materials and methods

2.1. Agents

Compound 21 is formulated as (S)-3 hydroxy-2-[(2,4,6-trimethoxybenzyl) amino] propanoic acid, which was synthesized by the Department of Pharmaceutical Chemistry, Institute of Materia Medica, Chinese Academy of Medical Science (Fig. 1A). It is a white powder with 99.9% purity. FTY720 was obtained from Novartis, Basel, Switzerland. For the *in vivo* experiments, Compound 21 and FTY720 were dissolved in 0.5% sodium carboxymethyl cellulose (Sigma-Aldrich, St. Louis, MO, USA). For the *in vitro* assays, Compound 21 was dissolved in dimethylsulfoxide (Sigma-Aldrich).

2.2. Animals

Female Lewis rats aged 6–8 weeks weighing 170–180 g and male C57BL/6 mice aged 8–10 weeks weighting 20–25 g were obtained from Beijing Vital River Laboratory Animal Technology Co. Ltd. (Beijing, China). All the animals were housed under a 12 h light/dark cycle and specific pathogen-free conditions with free access to water and food. All the animal experiments were carried out according to the guidelines of the Beijing Municipal Ethic Committee for the care and use of laboratory animals.

2.3. EAE induction and treatments

A total of 40 female Lewis rats were adapted to the conditions described above for 7 days before experimentation. Then, they were divided into the following four groups, consisting of 10 rats per group: Control group, EAE group, Compound 21 group, and FTY720 group. The EAE rat model was induced according to the standard accepted methods. Briefly, 30 rats were immunized by subcutaneous injections of 50 μg MBP (Sigma-Aldrich) and 100 μL phosphate-buffered saline emulsified with an equal volume of complete Freund's adjuvant (CFA; Sigma-Aldrich) into both legs. Simultaneously, the other 10 rats were injected with CFA (Sigma-Aldrich) without MBP, defined as the Control group. We designated the day of immunization as day 0 post-immunization. Additionally, 100 μL pertussis toxin (800 ng/100 μL; Sigma-Aldrich) were given on day 0 and day 2 by intraperitoneal (i.p.) injection. Meanwhile, the Control group rats were injected intraperitoneally with an equal volume of saline. Thereafter, rats received daily oral administration of Compound 21 (35 mg/kg) or FTY720 (1 mg/kg, Novartis) from day 9 to 16, defined as the Compound 21 group and FTY720 group, respectively. The EAE group rats were treated with the vehicle during this period. We calculated the dose of Compound 21 for the EAE rats based on our previous study of Compound 21 in CPZ mice [32]. The dose of FTY720 (1 mg/kg) was previously reported as effective in EAE rat models [33,34]. The animal treatment procedure is shown in Fig. 1B.

2.4. Clinical scores assessment

To evaluate neurological dysfunction, two investigators blinded to treatments performed daily the Knoz score test, which is based on the following criteria [33,35,36]: 0, normal, absence of symptoms; 0.5, partial loss of tail vitality, showing that the tail end cannot be curled; 1, tail paralysis; 2, paraparesis, hind limb weakness; 3, paraplegia, hind limb paralysis; 4, tetraparesis, hind limb paralysis, mild forelimb weakness and unable to recover after passive turning; 5, tetraplegia, complete paralysis of all the limbs or moribund; 6, death. The intermediate case was recorded as 0.5 points. In addition, all rats were weighed every day.

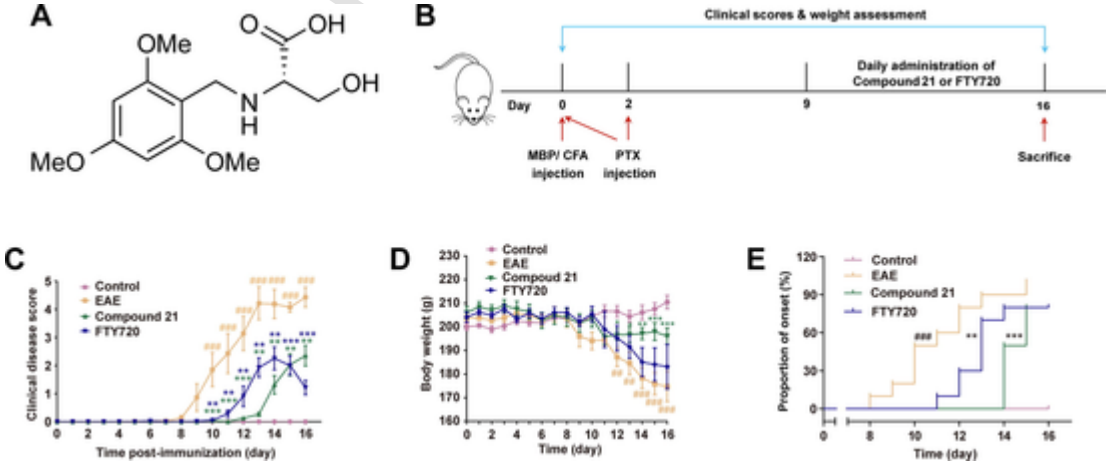

Fig. 1. Compound 21 treatment attenuated neurological deficits and body weight loss in experimental autoimmune encephalomyelitis (EAE) rats. (A) The chemical structure of Compound 21. (B) The flowchart of animal treatments. (C) Clinical scores of rats. (D) The body weights of rats. (E) The onset status of all the rats expressed by Kaplan-Meier Curve. MBP, myelin basic protein; CFA, complete Freund's adjuvant; PTX, pertussis toxin. Values are presented as the mean ± SD; n = 10 per group. $^{\#\#}P < 0.01$, $^{\#\#\#}P < 0.001$ versus the Control group; $^{*}P < 0.05$, $^{**}P < 0.01$, $^{***}P < 0.001$ versus the EAE group.

2.5. Cell culture

BV2 cells were obtained from the Cell Resource Center, IBMS, CAMS/PUMC (Beijing, China) and maintained in 90% Dulbecco's Modified Eagle Medium (DMEM; Solarbio, Beijing, China) supplemented with 10% fetal bovine serum (FBS; Gibco, Grand Island, NY, USA). BV2 cells were plated in 6-well plates at a density of 2×10^5 cells/well and kept in 5% CO_2 at 37 °C for 24 h.

Naïve $CD4^+$ T cells were isolated from spleens of 18 C57BL/6 mice using the MojoSort™ Mouse CD4 Naïve T Cell Isolation Kit (Biolegend, San Diego, CA, USA). The cells were cultured in 90% Iscove's Modified Dulbecco's Medium (IMDM; Gibco) containing 10% FBS (Gibco) at a density of 1×10^6 cells/well in 24-well plates.

2.6. Co-culture of $CD4^+$ T cells and BV2 cells

The BV2 cells were pretreated with or without the presence of Compound 21 (10 μM) for 1 h and then cultured in the absence or presence of lipopolysaccharides (LPS; 1 μg/mL, Sigma-Aldrich) for 24 h. Subsequently, the Naïve $CD4^+$ T cells were added to BV2 cells at a ratio of 4:1 (4×10^5 Naïve $CD4^+$ T cells, 1×10^5 BV2 cells) in the presence of MBP (5 μg/mL, Sigma-Aldrich) and ConA (5 μg/mL, Sigma-Aldrich). After 72 h of co-culture, the $CD4^+$ T cells were collected for flow cytometric analysis.

2.7. Hematoxylin & eosin staining

Three rats were randomly selected from each group and deeply anesthetized with 1% pentobarbital (40 mg/kg, i.p.), then they were perfused through the intracardiac route using saline infusion followed by 4% paraformaldehyde. The brains and lumbar spinal cords were obtained and fixed in 4% paraformaldehyde for 24 h. Next, the tissue samples were kept in 4% paraformaldehyde containing 30% sucrose. The brain and lumbar spinal cord tissues were embedded in paraffin and serially sliced at a 5-μm thickness. To assess inflammatory cell infiltration, the sections were stained with hematoxylin and eosin (H&E). The inflammatory infiltration was scored blindly by two observers as follows: 0, no inflammatory cells infiltration; 1, meningeal cells infiltration; 2, up to four small areas of perivascular cell infiltration; 3, five or more than five small areas of perivascular cell infiltration, and/or more than one large-scale cell infiltration; 4, a large number of cell infiltrations involving more than 20% of the white matter.

2.8. Luxol fast blue staining

To assess demyelination, the sections were processed as described above and stained with luxol fast blue (LFB). In brief, the tissue slides were incubated in LFB solution (0.1%) overnight at 60 °C. Then, the sections were differentiated in 0.05% lithium carbonate solution to distinguish the white matter from the gray matter. Finally, the sections were observed under a light microscope (Nikon E600, Tokyo, Japan). Demyelination in EAE rats was evaluated blindly by two investigators using the following scoring criteria: 0, no myelin loss; 1, a small range of myelin loss; 2, two or three small areas of myelin loss; 3, up to two large-scale myelin losses; 4, a large range of myelin loss involving more than 20% of the white matter.

2.9. Immunohistochemical staining

The tissue processing was the same as described above. Demyelination/remyelination or T-cell infiltration was assessed using immunohistochemical (IHC) staining of the brain. The sections were deparaffinized and rehydrated, then blocked in 3% bovine serum albumin and incubated overnight at 4 °C with the following primary antibodies: anti-MBP, anti-Olig2, anti-IFN-γ, and anti-IL-17 (1:300, Servicebio, Wuhan, China). Next, the sections were washed and incubated with goat anti-rabbit IgG–horseradish peroxidase (1:200, Servicebio) for 2 h at room temperature. The DAB reagent (Servicebio) was used to visualize positive cells. The sections were observed using a Carl Zeiss microscope (Jena, Germany), and the quantification of MBP, Olig2, IFN-γ, and IL-17 was analyzed by Image Pro Plus 6.0 software.

2.10. Co-immunofluorescence staining

The tissues were prepared as described above. The sections were deparaffinized and rehydrated. Subsequently, they were immersed in EDTA antigen retrieval buffer (pH, 8.0) and maintained at a sub-boiling temperature for 8 min. Next, we added 3% bovine serum albumin to block nonspecific binding for 30 min and incubated slides overnight at 4 °C with the following primary antibodies: anti-Iba-1 (1:500, Servicebio), anti-CD86 (1:200, Servicebio), and anti-CD206 (1:200, Servicebio). To visualize the immunostained cells, goat anti-mouse IgG-CY3 (1:300, Servicebio) and goat anti-rabbit IgG-Alexa Fluor 488 (1:400, Servicebio) were used; nuclei were stained using DAPI solution. The images were digitized using fluorescent microscopy (Nikon Eclipse C1, Tokyo, Japan). The cell numbers were analyzed using Image Pro Plus 6.0 software.

2.11. In vitro $CD4^+$ T-cell differentiation

Naïve $CD4^+$ T cells were seeded at a density of 1×10^6 cells/plate in 24-well plates and cultured in nonpolarizing (Th0) and polarizing (Th1 and Th17) conditions. For Th1-polarizing conditions, plate-bound anti-mouse CD3ε (3 μg/mL, Biolegend) and soluble anti-mouse CD28 (3 μg/mL, Biolegend) supplemented with mouse IL-12 (10 ng/mL, Biolegend), mouse IL-2 (5 ng/mL, Biolegend), and anti-mouse IL-4 (10 μg/mL, Biolegend) were used. For Th17-polarizing conditions, plate-bound anti-mouse CD3ε (3 μg/mL, Biolegend) and soluble anti-mouse CD28 (5 μg/mL, Biolegend) supplemented with mouse IL-6 (50 ng/mL, Biolegend), mouse TGF-β1 (1 ng/mL, Biolegend), and mouse IL-23 (5 ng/mL, Biolegend) were applied. $CD4^+$ T cells cultured in different polarizing conditions were treated with vehicle or Compound 21 (10 μM). After 96 h, Th1 and Th17 cells with different treatments were harvested and stimulated using a cell activation cocktail (with Brefeldin A) (2 μL/test, Biolegend) for 6 h.

2.12. In vitro $CD4^+$ T-cell proliferation assay

The BV2 cells were pretreated with or without the presence of Compound 21 (10 μM) for 1 h and then cultured in the absence or presence of LPS (1 μg/ml, Sigma-Aldrich) for 24 h. Subsequently, the Naïve $CD4^+$ T cells were added to BV2 cells at a ratio of 4:1 (4×10^5 Naïve $CD4^+$ T cells, 1×10^5 BV2 cells) in the presence of MBP (5 μg/mL, Sigma-Aldrich) and ConA (5 μg/mL, Sigma-Aldrich). After 72 h of co-culture, the $CD4^+$ T cells were collected for flow cytometric analysis.

2.13. In vitro $CD4^+$ T-cell apoptosis assay

Naïve $CD4^+$ T cells were plated in 24-well plates at a density of 1×10^6 cells/well and activated in different polarizing conditions with or without the presence of Compound 21 for 96 h. $CD4^+$ T cell apoptosis was measured using StarGlow Annexin V-FITC/PI Apoptosis Detection Kit (GenStar, Beijing, China). Briefly, the

cells were harvested and washed with cold PBS three times, and then they were resuspended in 100 μL Annexin V-FITC Binding Buffer followed by rh Annexin V-FITC (5 μL/test) for 5 min at RT in the dark. 10 μL/test PI (20 μg/mL) and 400 μL/test PBS were added and the flow cytometry was performed immediately.

2.14. Quantitative polymerase chain reaction assay

For *in vivo* experiments, the total RNA was extracted from the brain or lumbar spinal cord tissues using the TransZol Up Plus RNA kit (TransGen Biotech Co., Beijing, China) in accordance with the manufacturer's protocol. Then, identical amounts of RNA were reversed into cDNA using TransScript One-Step gDNA Removal and cDNA Synthesis SuperMix (TransGen Biotech Co.) following the manufacturer's instructions. Quantitative polymerase chain reaction assay (qPCR) of different genes was conducted using TransStart Tip Green qPCR SuperMix (+DyeI/+ DyeII) (TransGen Biotech Co.). For *in vitro* experiments, BV2 cells were preincubated with Compound 21 (10 μM) for 1 h, then stimulated with LPS (1 μg/mL, Sigma-Aldrich) for 6 h. Subsequently, the total RNA was harvested from induced BV2 cells, and the subsequent steps were the same as described above. The mRNA was amplified for PCR with the sets of primers shown in Tables 1 and 2. PCR amplification was run in the 7900HT Fast Real-Time PCR system (Applied Biosystems, Foster City, CA, USA) with the following thermocycler conditions: stage 1, 94 °C for 30 sec for one cycle; stage 2, 94 °C for 5 sec, 59 °C for 15 sec, and 72 °C for 10 sec for 40 cycles; stage 3, 95 °C for 15 sec and 60 °C for 15 sec for one cycle. The relative quantification of mRNA expression was calculated by −ΔΔCt algorithms.

2.15. Enzyme-linked immunosorbent assay

After anesthetizing the rats with 1% pentobarbital (40 mg/kg, i.p.), we quickly collected blood samples from the abdominal aorta in serum separator tubes. Next, the samples were allowed to clott for 2 h at room temperature and were centrifugated at 1000 × g for 20 min. IL-17 and IFN-γ concentrations were measured by IL-17 and IFN-γ enzyme-linked immunosorbent assay (ELISA) kits following the protocol recommended by the supplier (Jianglai Industrial Limited By Share Ltd, Shanghai, China). Briefly, we added 50 μL of each sample to the appropriate wells and incubated the microtiter plate at 37 °C for 30 min. Next, we added 100 μL enzyme conjugate to each well and incubated at 37 °C for 60 min. Then, the microtiter plate was washed four times, and 50 μL Substrate A and 50 μL Substrate B were added to each well and incubated at 37 °C for 15 min. Finally, 50 μL stop solution was applied to each well, and the optical density was detected at 450 nm. The cytokine concentrations were calculated by standard protein concentration.

2.16. Flow cytometry analysis

For *in vivo* experiments, cells were isolated from the spleen and plated in 24-well plates at a density of 1×10^6 cells/well. Then, the cells were treated with a cell activation cocktail (2 μL/well, Biolegend) containing ionomycin, phorbol myristate acetate, and Gol-

Table 1
Primers used for quantitative PCR in rat tissues.

Gene	Primer sequence(5′-3′)	
	Forward	Reverse
Ifng	GAGGTGAACAACCCACAGA	TATTGGCACACTCTCTACCC
Il23	CACCTGCTGGACTCGGACAT	CTGCGAAGGATCTTGGAACG
Il1b	TGATGTTCCCATTAGACAGC	GAGGTGCTGATGTACCAGTT
Tnf	AAGCCCGTAGCCCACGTCGTA	GCCCGCAATCCAGGCCACTAC
Il12a	CTCTTCTTGGCCACCCTTGT	CATGTCGTCCGTGGTCTTCA
Il17a	TGAAGGCAGCGGTACTCATC	GGGTGAAGTGGAACGGTTGA
Gapdh	AGTGCCAGCCTCGTCTCATA	GGTAACCAGGCGTCCGATAC

Table 2
Primers used for quantitative PCR in BV2 cells.

Gene	Primer sequence(5′-3′)	
	Forward	Reverse
Tnf	ACGGCATGGATCTCAAAGAC	AGATAGCAAATCGGCTGACG
Nos2	CAGCTGGGCTGTACAAACCTT	CATTGGAAGTGAAGCGTTTCG
Il23	CCAGCAGCTCTCTCGGAATC	CAGACCTTGGCGGATCCTTT
Cd16	TATCGGTGTCAAATGGAGCA	GCACCTTAGCGTGATGGTTT
Cd32	AATCCTGCCGTTCCTACTGATC	GTGTCACCGTGTCTTCCTTGAG
Arg1	TGAACACGGCAGTGGCTTTA	GTAGTCAGTCCCTGGCTTATGG
Ifng	ACGGCACAGTCATTGAAAGCCTAGA	TGTCACCATCCTTTTGCCAGTTCC
Il12a	AAATGAAGCTCTGCATCCTGC	TCACCCTGTTGATGGTCACG
Il6	CCTACCCCAATTTCCAATGCT	TATTTTCTGACCACAGTGAGGAAT
Cd206	GGATAGATGGAGGGTGCGGTA	GGTTCAGTAGCAGGGATTTCGT
Cd86	TGTTTCCGTGGAGACGCAAG	CAGCTCACTCAGGCTTATGTTTT
Tgfb1	GCCCGAAGCGGACTACTATG	TGCTTCCCGAATGTCTGACG
Il10	ACTTGGGTTGCCAAGCCTTA	AGAAATCGATGACAGCGCCT
Gapdh	ATGACTCTACCCACGGCAAG	GATCTCGCTCCTGGAAGATG

giStop for 6 h in 5% CO_2 at 37 °C. For surface staining, the cells were incubated with FITC mouse anti-rat CD4 (2 μL/test, BD Biosciences, Franklin Lakes, NJ, USA) for 30 min at 4℃. Subsequently, they were permeabilized and fixed using the Cytofix/Cytoperm Fixation/Permeabilization solution kit (250 μL/test, BD Biosciences) for intracellular staining. Fc receptors were blocked with 5% FBS (Gibco), and the cells were stained with PE mouse anti-rat IFN-γ (20 μL/test, Biolegend), APC mouse anti-rat IL-17A (0.625 μL/test, BD Biosciences) and appropriate isotype-matched controls for 30 min at 4 ℃, then analyzed using a BD FACS Canto II flow cytometer (BD Biosciences).

For *in vitro* experiments, the BV2 cells were seeded at a density of 2×10^6/well in 6-well plates and treated with LPS (1 μg/mL, Sigma-Aldrich) for 24 h (LPS group). For the LPS + Compound 21 group and LPS + IL-4 group, cells were pretreated with Compound 21 (10 μM) or IL-4(10 ng/mL, ProTech, Rocky Hill, NJ, USA) for 1 h and then treated with LPS (1 μg/mL, Sigma-Aldrich) for 24 h. The cells were harvested and blocked by anti-mouse CD16/32 (2 μL/test, Biolegend) and incubated with Alexa Fluor 488 anti-mouse CD86 antibody (4 μL/test, Biolegend). Then, they were permeabilized and fixed for intracellular staining using Alexa Fluor 647 anti-mouse CD206 (MMR) antibody and Alexa Fluor 647 Rat IgG2a, κ Isotype Ctrl Antibody (2 μL/test, Biolegend) for 30 min at 4℃. The subsequent staining steps were performed as described above. A final acquisition of stained cells was carried out using an ImageStreamX imaging flow cytometer (Amnis, Seattle, WA, USA).

Flow cytometry was also used to detect $CD4^+$ T-cell differentiation *in vitro*. Naïve $CD4^+$ T cells were treated in different conditions and collected after being stimulated with cell activation cocktail (with Brefeldin A) (2 μL/test, Biolegend) for 6 h. Then, cells were surface-labeled with FITC anti-mouse CD4 antibody (1 μL/test, Biolegend) for 30 min at 4 ℃. For the intracellular staining, cells were permeabilized and fixed. Fc receptors were blocked with anti-mouse CD16/32 (2 μL/test, Biolegend), and the cells were incubated with PE anti-mouse IFN-γ antibody (1.25 μL/test, Biolegend), APC anti-mouse IL-17A antibody (1.25 μL/test, Biolegend), and appropriate isotype-matched controls for 30 min at 4 ℃. The samples were analyzed using the BD FACS Canto II flow cytometer (BD Biosciences).

2.17. Statistical analysis

We conducted the statistical analysis using SPSS version 20.0 software. Data were presented as the means ± standard deviation. Multiple comparisons were performed by one-way analysis of variance, followed by the least significant difference test. For clinical and histological scores and cell numbers, the Kruskal-Wallis test was used, followed by the Mann-Whitney *U* test. Log-rank analysis was conducted to compare the incidences of different groups. The independent *t* test was applied to two-group comparisons. P values < 0.05 were considered statistically significant.

3. Results

3.1. Compound 21 treatment alleviates neurological deficits and body weight loss in EAE rats

Body weight loss and neurological dysfunction are commonly witnessed in EAE rats. To evaluate the protective effect of Compound 21 on EAE rats, female Lewis rats were immunized with MBP peptide, and two groups were fed Compound 21 or FTY720 from day 9 post-immunization (Fig. 1B). In this study, rats in the EAE group started to show severe MS symptoms on day 11 (11.00 ± 2.05) post-immunization. By contrast, only 80% of the rats fed with Compound 21 showed much slighter symptoms. Moreover, Compound 21 treatment prominently delayed the onset of EAE symptoms to day 15 (14.70 ± 0.82; $P < 0.01$) (Table 3 and Fig. 1E). As illustrated in Fig. 1C, the clinical scores of the EAE group peaked on day 13. Compound 21 treatment remarkably deceased the maximum clinical scores (EAE group, 5.11 ± 0.93; Compound 21 group, 2.6 ± 1.15; $P < 0.001$) and significantly reduced the mean scores (EAE group, 1.36 ± 0.54; Compound 21 group, 0.36 ± 0.17; $P < 0.001$). Compound 21 showed comparable protective effects on clinical scores as FTY720 (Table 3; Fig. 1C and E). In general, EAE rats treated with Compound 21 showed remarkably lower disease incidence, delayed onset, and lower clinical scores compared to vehicle-treated EAE animals. Correspondingly, the EAE group showed significantly lower body weight than the Control group. However, Compound 21 treatment remarkably attenuated the weight loss in EAE rats (Fig. 1D). Together, these data suggest that Compound 21 treatment alleviates neurological deficits and body weight loss in EAE rats.

3.2. Compound 21 alleviates pathological features in EAE rats

MS is pathologically characterized by immune infiltration and demyelination in the CNS. Characteristic infiltration of inflammatory cells was detected in the spinal cord and brain of EAE rats using H&E staining. In the spinal cord, Compound 21 treatment decreased the histological score of inflammation from 3.67 in the EAE group to 0.78 in the Compound 21 group ($P < 0.001$). Consistently, Compound 21 administration reduced the score from 3.89 to 1.00 in the brain ($P < 0.001$) (Fig. 2A–C). In addition, LFB staining revealed that Compound 21 treatment protects the spinal cord ($P < 0.001$) and the brain ($P < 0.01$) from demyelination (Fig. 2D–F). Olig2 and MBP, the markers representing oligodendrocytes and myelin sheaths, respectively, were tested using IHC to further determine the myelin status in EAE rats. As shown in Fig. 2G–I, the brains of the EAE group showed fewer Olig2-positive cells and lower MBP expression than those of the Control group. Compound 21 treatment protected Olig2-positive cells (EAE group, 544 cells/mm^2; Compound 21 group, 944 cells/mm^2; $P < 0.05$) and preserved MBP expression in the brain of EAE rats ($P < 0.001$), suggesting Compound 21 attenuates myelin damage. However, the FTY720 group rats showed no differences in Olig2 and MBP expression compared with the EAE group rats (Fig. 2G–I).

Table 3
Clinical features of experimental autoimmune encephalomyelitis (EAE) rats by group.

Group	Number of rats	Incidence	Disease onset (days p.i.)	Maximum clinical score	Mean clinical score
Control	10	0	–	0	0
EAE	10	100%	11.00 ± 2.05 ###	5.11 ± 0.93 ###	1.36 ± 0.54 ###
Compound 21	10	80%	14.70 ± 0.82**	2.6 ± 1.15***	0.36 ± 0.17***
FTY720	10	80%	13.30 ± 1.64*	2.41 ± 1.18***	0.51 ± 0.30**

Abbreviations: p.i., post-immunization.
Values are presented as the means ± SD. ###$P < 0.001$ versus Control rats. *$P < 0.05$, **$P < 0.01$, ***$P < 0.001$ versus EAE rats.

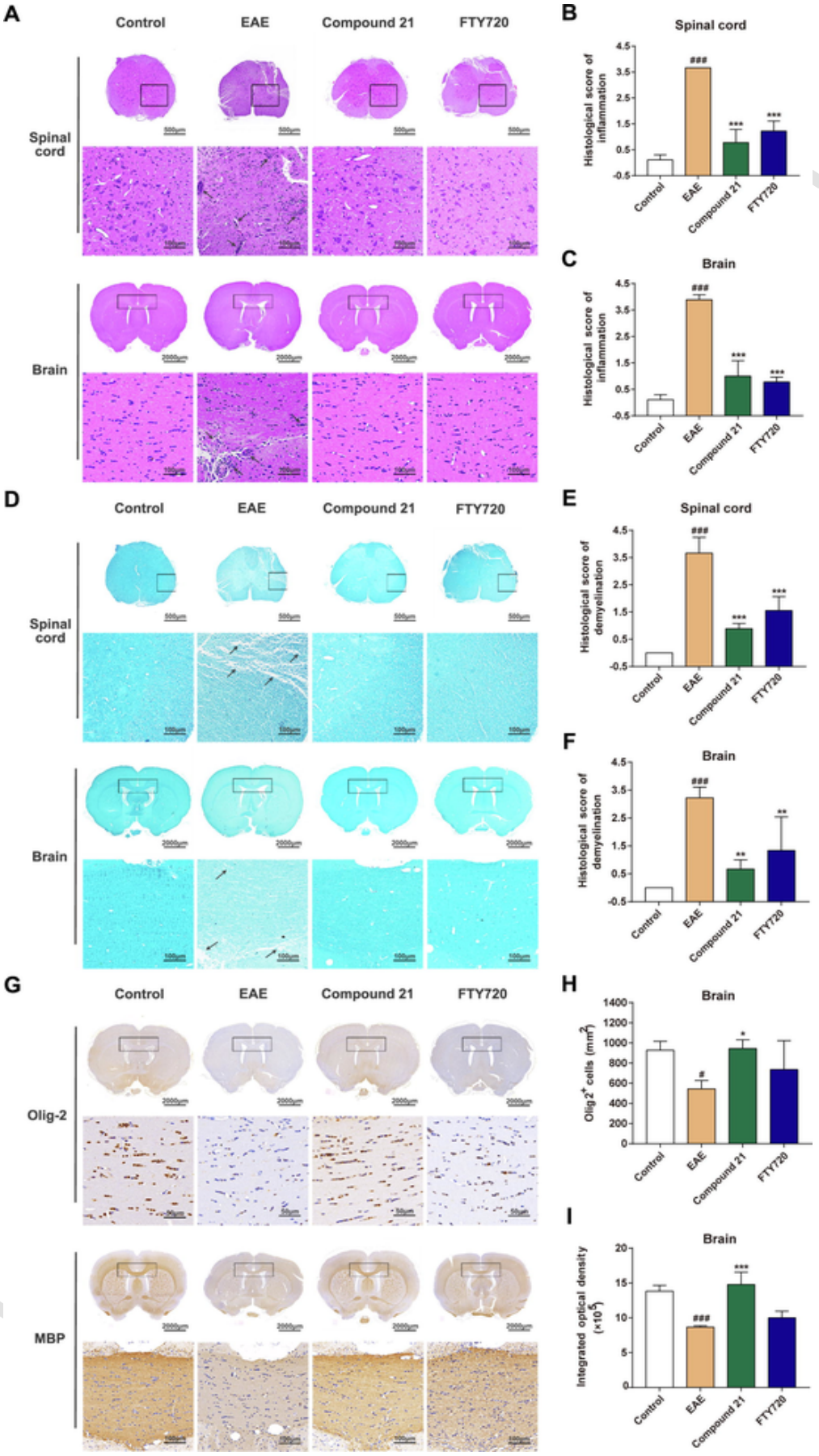
A
Control
EAE
Compound 21
FTY720
Spinal cord
Brain
B
Spinal cord
Histological score of inflammation
C
Brain
Histological score of inflammation
D
Control
EAE
Compound 21
FTY720
Spinal cord
Brain
E
Spinal cord
Histological score of demyelination
F
Brain
Histological score of demyelination
G
Control
EAE
Compound 21
FTY720
Olig-2
MBP
H
Brain
Olig2+ cells (mm2)
I
Brain
Integrated optical density (×10^5)

Fig. 2.

Compound 21 treatment alleviated pathological features of experimental autoimmune encephalomyelitis (EAE) rats. (A) Representative images of H&E staining in the spinal cord and brain; black arrows indicate perivascular cuffing and inflammatory infiltration. Statistical analysis of inflammatory cell infiltration in the (B) spinal cord and (C) brain. (D) Representative images of LFB staining in the spinal cord and brain; black arrows point to areas of demyelination. Statistical analysis of LFB staining of the (E) spinal cord and (F) brain. (G) Representative images of IHC staining of Olig2 and MBP in the brain. Statistical analysis of IHC staining of (H) Olig2 and (I) MBP. Black squares indicate the positions of high magnification fields. All brain and spinal cord tissues were collected on day 16 post-immunization. MBP, myelin basic protein. Values are presented as the mean ± SD; n = 3 per group (3 sections per rat). $^{\#}P < 0.05$, $^{\#\#\#}P < 0.001$ versus the Control group; $^{*}P < 0.05$, $^{***}P < 0.001$ versus the EAE group.

These data indicate that Compound 21 treatment inhibits immune infiltration and attenuates demyelination in EAE rats.

3.3. Compound 21 treatment reduces Th1/Th17 cell population and infiltration in EAE rats

In the pathogenesis of MS, Th1 and Th17 cells differentiate from $CD4^+$ T cells in the periphery [25,37], then invade the CNS and damage myelin sheaths [7]. To determine whether the improvement in EAE rats by Compound 21 was related to its suppression on the Th1/Th17 cell population, we detected the percentages of Th1 and Th17 cells in the periphery using flow cytometry. As shown in Fig. 3A–D, the spleens of EAE rats exhibited remarkably higher percentages of Th1 and Th17 cells (both $P < 0.01$). The Compound 21 group showed a significantly lower percentage of Th1 cells than the EAE group (EAE group, 5.03%; Compound 21 group, 1.91%; $P < 0.01$). For Th17 cells, the percentage declined in the Compound 21 group compared with that of the EAE group (EAE group, 2.57%; Compound 21 group, 0.98%; $P < 0.01$). In addition, the EAE group showed higher levels of serum IFN-γ and IL-17 (the representative cytokines produced by Th1 and Th17 cells, respectively) as detected by ELISA. Consistent with decreased splenic Th1 and Th17 cells, the Compound 21 group exhibited lower levels of serum IFN-γ (EAE group, 65.85 pg/mL; Compound 21 group, 52.67 pg/mL; Fig. 3E) and IL-17 (EAE group, 40.49 pg/mL; Compound 21 group, 34.74 pg/mL; Fig. 3F) than the EAE group (both $P < 0.001$). According to qPCR results of spinal cord and brain tissues, the expression of *Ifng* and *Il17a* were higher in the EAE group and lower in the Compound 21 group (Fig. 3J–K). From IHC analysis, IFN-γ-positive (Th1) cells ($P < 0.01$) and IL-17–positive (Th17) cells ($P < 0.001$) were higher in the EAE group rats than the Control group. Compound 21 treatment re-

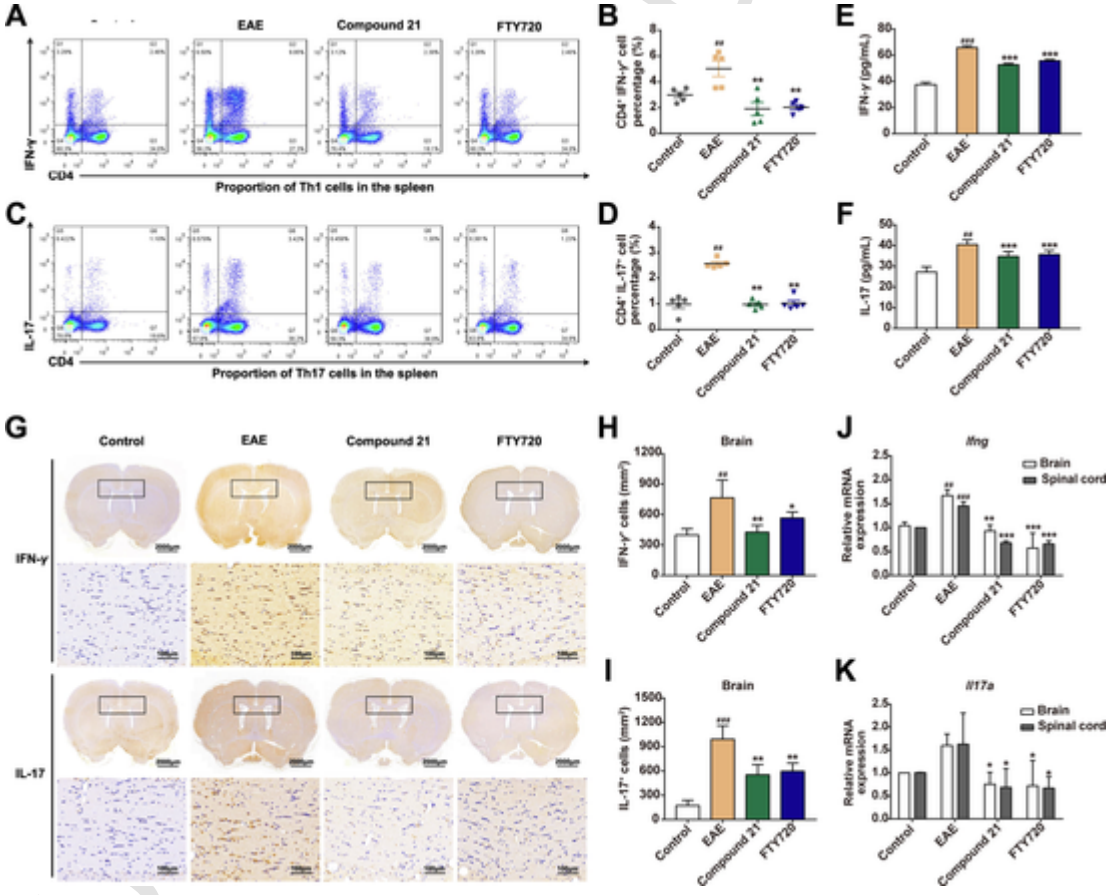

Fig. 3. Compound 21 treatment decreased Th1/Th17 cell population and infiltration in experimental autoimmune encephalomyelitis (EAE) rats. Flow cytometric analysis of (A and B) IFN-γ and (C and D) IL-17 expression in the spleens of rats. Expression of (E) IFN-γ and (F) IL-17 in the serum of rats detected by ELISA. (G) Representative IHC staining images of IFN-γ and IL-17 in the brain. Statistical analysis of IHC staining of (H) IFN-γ and (I) IL-17. The mRNA expression of (J) *Ifng* and (K) *Il17a* detected by qPCR in the CNS. Black squares indicate the positions of high magnification fields. All splenic cells, tissues, and serum were collected on day 16 post-immunization. Values are presented as the mean ± SD; n = 5 per group for flow cytometric analysis and ELISA analysis; n = 3 per group (3 sections per rat) for IHC analysis. $^{\#\#}P < 0.01$, $^{\#\#\#}P < 0.001$ versus the Control group; $^{*}P < 0.05$, $^{**}P < 0.01$, $^{***}P < 0.001$ versus the EAE group.

duced the numbers of Th1 cells (EAE group, 765 cells/mm^2; Compound 21 group, 427 cells/mm^2; $P < 0.01$) and Th17 cells (EAE group, 993 cells/mm^2; Compound 21 group, 553 cells/mm^2; $P < 0.01$) in the brain (Fig. 3G–I), indicating Compound 21 effectively inhibits the infiltration of Th1/Th17 cells. For all the above-mentioned effects, Compound 21 showed similar potency to FTY720. These results suggest that Compound 21 inhibits the Th1/Th17 cell population and infiltration, contributing to its protective effect.

3.4. Compound 21 influences CD4$^+$ T cells by directly inhibiting Th1/Th17 differentiation in vitro

To explore whether Compound 21 inhibits Th1/Th17 cell population and infiltration in EAE rats by directly suppressing Th1 and Th17 cells, we isolated and purified naïve CD4$^+$ T cells from mice spleens, then cultured them under nonpolarizing (Th0) and polarizing (Th1/Th17) conditions with or without the presence of Compound 21 (10 μM) *in vitro*. Flow cytometric analyses were performed to detect the effects of Compound 21 on the proliferation, apoptosis and differentiation of Th1/Th17 cells. No differences in apoptosis (Fig. 4A–D) and proliferation (Fig. 4I–K) were shown between the CD4$^+$ T cells in the Compound 21 group and those of the vehicle group, suggesting these factors are not affected by Compound 21. However, the differentiation of Th1/Th17 cells was significantly influenced by Compound 21. The percentage of IFN-γ-positive (Th1) T cells elevated from 9.12% in the Th0 condition to 11.57% in the Th1-ploarizing condition ($P < 0.05$); however, Compound 21 (10 μM) treatment reduced the percentage of Th1 cells to 8.07% ($P < 0.01$) (Fig. 4E–F). In the Th17-polarizing condition, Compound 21 treatment reduced the frequency of Th17 cells from 15.23% to 12.10% ($P < 0.05$), which was still higher than that in the Th0 condition (Fig. 4G–H). These results suggested that Compound 21 directly inhibits Th1 differentiation and influences Th17 differentiation. Therefore, the suppressive effects of Compound 21 on Th1/Th17 cell population and infiltration were partially mediated by its direct influence on the differentiation of Th1/Th17 cells rather than proliferation or apoptosis.

3.5. Compound 21 treatment inhibits proinflammatory microglial cells to suppress Th1/Th17 cell differentiation and stabilization

Of the glial cells in the CNS, proinflammatory microglial cells are believed to play a key role in EAE development [38]. Many cytokines generated by proinflammatory microglial cells, including IL-12, IFN-γ, and TNF-α, could induce naïve CD4$^+$ T cells to differentiate into Th1 cells. Several other proinflammatory molecules such as TGF-β, IL-6, IL-1β, and IL-23 are involved in Th17 cell differentiation [38]. Some of these cytokines are also responsible for maintaining the stabilization of infiltrated Th1/Th17 cells [39]. Once the levels of these cytokines are reduced, the differentiation and stabilization of infiltrated Th1/Th17 cells in the CNS would be disturbed. Therefore, we hypothesized that inhibiting microglial cells from producing proinflammatory cytokines in the CNS was involved in the suppressive effect of Compound 21 on infiltrated Th1/Th17 cells. To verify the hypothesis, naïve CD4$^+$ T cells were co-cultured with BV2 cells, a mouse microglial cell line. In brief, BV2 cells were pretreated with Compound 21 (10 μM) or the vehicle, then stimulated by LPS to mimic the induction of proinflammatory microglial cells. Next, we added naïve CD4$^+$ T cells to the BV2 cells with different treatments and co-cultured for 72 h. Finally, CD4$^+$ T cells were analyzed using flow cytometry. The re-

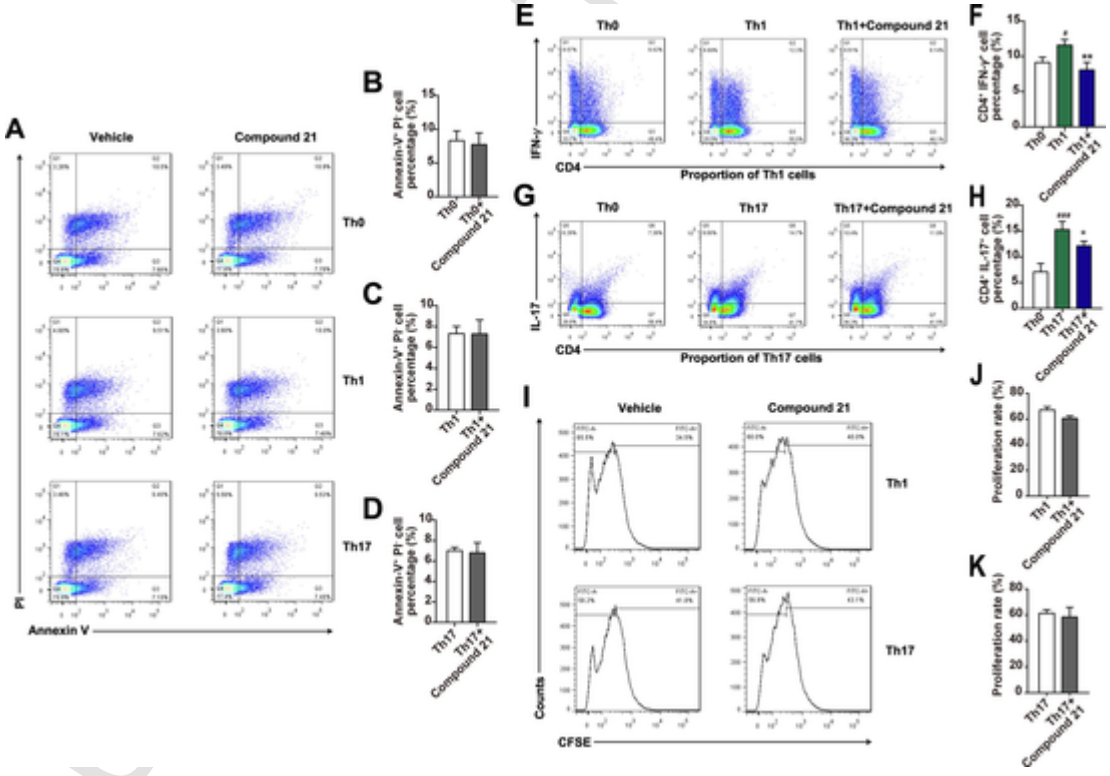

Fig. 4. Compound 21 treatment inhibited Th1/Th17 cell differentiation *in vitro*. (A) Flow cytometric analysis of CD4$^+$ T-cell apoptosis in different polarizing conditions. The percentages of annexin-V$^+$PI$^-$ cells regarded as apoptotic cells in (B) nonpolarizing, (C) Th1-polarizing, and (D) Th17-polarizing conditions. Flow cytometric analysis of (E and F) Th1 (IFN-γ^+ CD4$^+$) cells and (G and H) Th17 (IL-17$^+$ CD4$^+$) cells in different polarizing conditions *in vitro*. (I) Cell proliferation of CD4$^+$ T cells in Th1 and Th17 polarizing conditions by CFSE staining. Statistical analysis of proliferation rates in (J) Th1 and (K) Th17 polarizing conditions. Values are presented as the mean ± SD; n = 5 per group for cell apoptosis and cell proliferation analysis; n = 3 per group for CD4$^+$ T-cell differentiation analysis. $^{\#}P < 0.05$, $^{\#\#\#}P < 0.001$ versus nonpolarizing cells; $^{*}P < 0.05$, $^{**}P < 0.01$ versus polarizing cells.

sults showed that Compound 21 significantly reduced the percentages of Th1 cells (from 18.97% to 9.16%; $P < 0.001$) (Fig. 5A and B) and Th17 cells (from 8.40% to 5.47%; $P < 0.05$) (Fig. 5A–C), indicating that suppressing proinflammatory microglial cells are involved in inhibiting Th1/Th17 cell differentiation in the CNS.

To further determine whether the suppressive effects of Compound 21 treatment in the co-culture system were mediated by influencing the levels of cytokines produced by proinflammatory microglial cells, we tested the expression of these related cytokines both *in vivo* and *in vitro* using qPCR. In both the spinal cord and brain, *Il12a* levels were elevated in EAE rats ($P < 0.05$) and reduced after treatment with Compound 21 ($P < 0.05$) (Fig. 5D). Similarly, Compound 21 treatment significantly suppressed *Il23* levels in the spinal cord ($P < 0.001$) and the brain ($P < 0.01$) of EAE rats (Fig. 5E). IL-23 was reported to be important for Th17 stabilization in the CNS, so we speculated that Compound 21 treatment might inhibit proinflammatory microglial cells from producing IL-23 to interfere with Th17 cell stabilization. The striking alteration of *Il1b* levels in the spinal cord of EAE rats ($P < 0.001$) indicates that IL-1β may play a critical role in the development of EAE (Fig. 5F). In addition, Compound 21 illustrated inhibitory effects on the production of these cytokines comparable to FTY720.

For the cytokine detection *in vitro,* we directly pretreated BV2 cells with the vehicle or Compound 21 (10 μM). Then, the cells were stimulated by LPS to detect the levels of proinflammatory cytokines using qPCR. Consistent with the results *in vivo*, Th1-related cytokines including *Il12a* ($P < 0.01$), *Ifng* ($P < 0.01$), and *Tnf* ($P < 0.001$) decreased remarkably after treatment with Compound 21 *in vitro* (Fig. 5G–I). As shown in Fig. 5J–L, Th17-related cytokines such as *Il6*, *Il23*, and *Tgfb1* were also downregulated after Compound 21 treatment ($P < 0.01$). All the evidence suggested that Compound 21 treatment directly inhibits proinflammatory microglial cells from producing cytokines responsible for Th1/Th17 cell differentiation and stabilization. These effects contribute to reducing the infiltrated Th1/Th17 cells in the CNS.

3.6. Compound 21 treatment suppressed proinflammatory microglial cells by switching M1/M2 polarization both in vivo and in vitro

Scientists have reported that resident microglia could be activated into two phenotypes: proinflammatory M1 or alternative M2. Microglial cells of the M1 phenotype were found to be involved in the development of EAE, and a switch from M1 to the M2 phenotypes was shown to alleviate the disease [40]. To further investigate whether Compound 21 treatment inhibited proinflammatory microglial cells from generating cytokines essential for Th1/Th17 cell differentiation and stabilization via modulating M1/M2 polarization, we assessed the microglial phenotypes among different groups both *in vivo* and *in vitro* using immunofluorescence, flow cytometry, and qPCR. The corpus callosum region was immunostained with CD86 as the M1 marker, CD206 as the M2 marker, and Iba-1 as the marker of total microglia. The EAE group exhibited a higher number of cells co-expressing CD86 and Iba-1 (M1 microglia) than the Control group ($P < 0.001$). After the administration of Compound 21, the numbers of double positive cells decreased ($P < 0.001$) (Fig. 6A–D). Meanwhile, the EAE group had fewer cells co-expressing CD206 and Iba-1 (M2 microglia) than the Control group ($P < 0.01$). After Compound 21 administration, the percentage of M2 microglial cells significantly increased ($P < 0.001$) (Fig. 6E–H), indicating Compound 21 suppresses M1 microglial cells and converts them into the M2 phenotype.

An *in vitro* experiment was also conducted. IL-4, a classic inducer of M2 microglial cells, was used to stimulate BV2 cells into the M2 phenotype [41,42]. As shown in the flow cytometry results, a higher expression of CD86 and a lower expression of CD206 were witnessed in LPS-induced BV2 cells, indicating LPS triggers M1 activation. Compound 21 treatment decreased CD86 expression and increased CD206 expression similar to IL-4 administration, suggesting that Compound 21 administration converts BV2 cells from the M1 phenotype to the M2 phenotype (Fig. 7A–D). Consistent with the results from flow cytometry, the increase in M2 markers (*Cd206*, *Arg1*, and *Il10*) and the decrease in M1 markers (*Cd86* and *Nos2*) in BV2 cells treated with Compound 21 were confirmed by qPCR (Fig. 7E–I). These *in vivo* and *in vitro* results suggest that Compound 21 treatment can convert microglial cells from the M1 phenotype to the M2 phenotype, contributing to the inhibition of cytokine generation essential for Th1/Th17 cell differentiation and stabilization in the CNS.

4. Discussion

Compound 21 is a phloroglucinol derivative with anti-inflammatory properties, as confirmed both *in vivo* and *in vitro* by our previous studies [30,31]. The hit compound of phloroglucinol derivatives, 3-methyl-1-(2,4,6-trihydroxyphenyl) butan-1-one, was isolated from *Lysidice rhodostegia* roots. We performed structural modification and optimization to improve its stability and enhance its pharmacological effects. Altogether, 43 compounds including Compound 21 were derived. Then, these derivatives were screened by anti-inflammatory activity experiments, and four top compounds were chosen for further pharmacokinetic properties and safety evaluation. Compound 21 exhibited potent anti-neuroinflammatory effects, good blood–brain barrier penetration, and desirable safety margins, suggesting that this compound would be a potential candidate in neuroinflammatory diseases such as MS. Further mechanistic studies revealed this neuroinflammation inhibition may be related to the Src/PTEN/Akt and Kalirin signaling pathways. However, it has yet to be determined whether Compound 21 interacts with a specific receptor or inespecific diffusion. A preliminary study in our laboratory showed that Compound 21 alleviated demyelination in an CPZ-intoxicated mouse model [32].

The current study demonstrated for the first time that Compound 21 treatment effectively alleviates the clinical signs and pathological features of EAE rats. Further studies suggest that Compound 21 treatment reduces the population of Th1/Th17 cells and inhibits their infiltration to alleviate demyelination in EAE rats. These effects partially resulted from the direct inhibition of Th1/Th17 cell differentiation by Compound 21 treatment. In addition, Compound 21 reduced the neuroinflammatory cytokines produced by proinflammatory microglia via switching M1/M2 polarization. In this way, Compound 21 affected the infiltrated Th1/Th17 cell differentiation and stabilization in the CNS.

The EAE rat model immunized with MBP is an animal model widely used to mimic the initiation and development of MS. Similar to MS, active EAE is characterized by acute T-cell inflammation and minimal primary demyelination [43]. After immunization, antigen-presenting cells recognize the injected antigens and interact with T cells in the spleen or lymph nodes, triggering the activation of pathogenic Th1 and Th17 cells. These pathogenic T cells infiltrate across the blood–brain barrier and promote inflammation and demyelination locally in the CNS [44]. The present study successfully established the EAE rat model to further estimate the effect of Compound 21 on MS and investigate the underlying mechanisms. FTY720, which exerts its effect via modulating sphingosine-1-phosphate (S1P)-receptor (S1PR), is the first oral agent approved by FDA for MS treatment [45]. Extensive experiments revealed that the immunosuppressive effects of FTY720 was mediated by its critical effects on T and B cell trafficking via impairment of S1PR1-associated recirculation, leading to significantly decreased lymphocyte in the blood and accumulation of lymphocyte in lymphoid tissues [46–48]. Here in the current study, we applied FTY720 as the positive control agent.

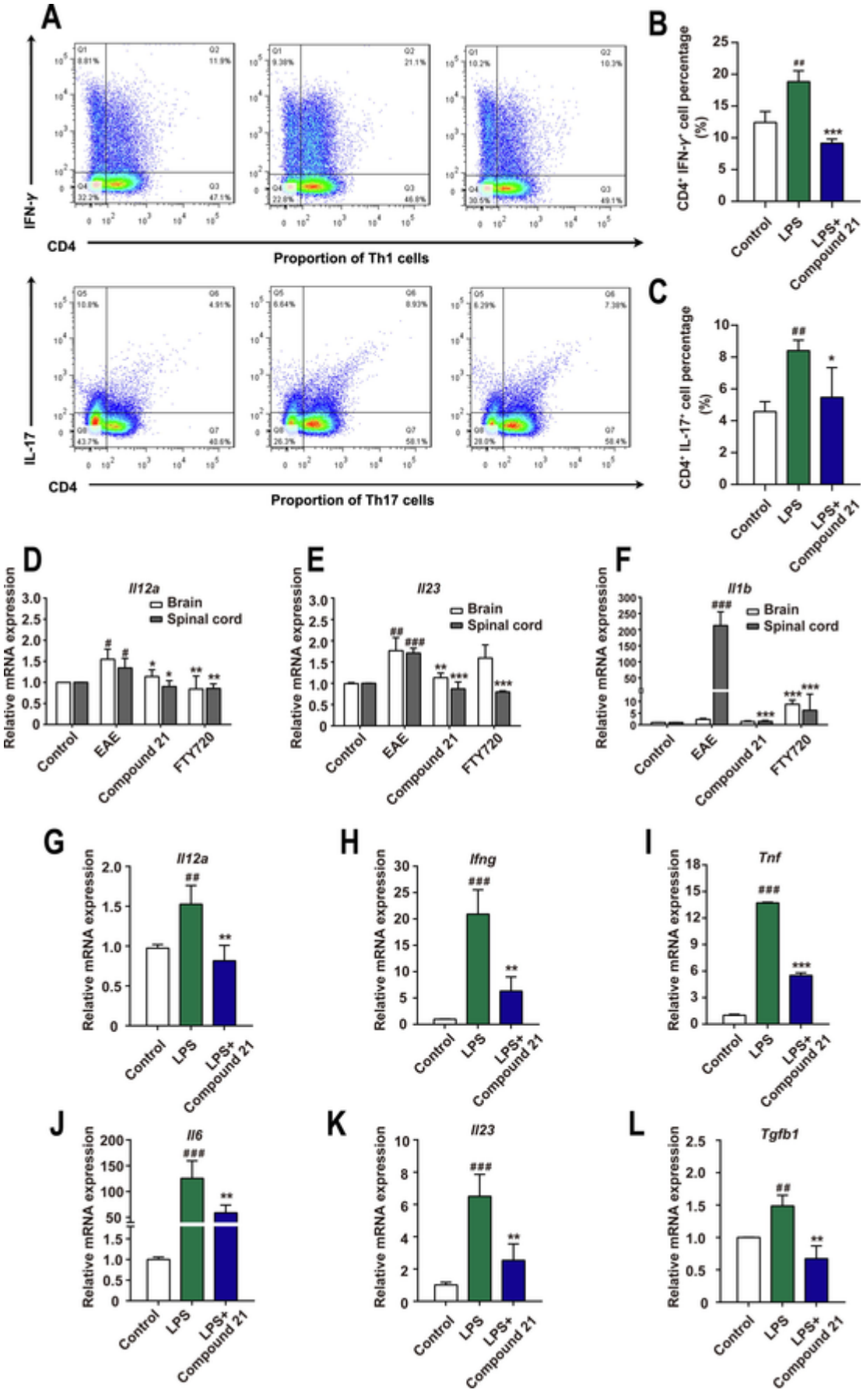
A
IFN-γ
CD4
Proportion of Th1 cells
B
CD4+ IFN-γ+ cell percentage (%)
Control
LPS
LPS+ Compound 21
IL-17
CD4
Proportion of Th17 cells
C
CD4+ IL-17+ cell percentage (%)
D
Il12a
Brain
Spinal cord
Relative mRNA expression
Control
EAE
Compound 21
FTY720
E
Il23
F
Il1b
G
Il12a
H
Ifng
I
Tnf
J
Il6
K
Il23
L
Tgfb1

Fig. 5.

Compound 21 treatment inhibited proinflammatory microglial cells to suppress Th1/Th17 cell differentiation and stabilization. (A) Flow cytometric analysis of Th1 (IFN-γ^+ CD4$^+$) cells and Th17 (IL-17$^+$ CD4$^+$) cells co-cultured with BV2 cells *in vitro*. Statistical analysis of percentages of (B) Th1 (IFN-γ^+ CD4$^+$) cells and (C) Th17 (IL-17$^+$ CD4$^+$) cells co-cultured with BV2 cells treated with vehicle or Compound 21. mRNA expression of cytokines in the spinal cord and brain of EAE rats: (D) *Il12a* expression, (E) *Il23* expression, and (F) *Il1b* expression. mRNA expression of cytokines in BV2 cells: (G) *Il12a* expression, (H) *Ifng* expression, (I)*Tnf* expression, (J) *Il6* expression, (K) *Il23* expression, and (L) *Tgfb1* expression. All the brain and spinal cord tissues were collected on day 16 post-immunization. LPS, lipopolysaccharides. Values are shown as the mean ± SD; n = 3 per group. $^{\#}P < 0.05$, $^{\#\#}P < 0.01$, $^{\#\#\#}P < 0.001$ versus the Control group. $^{*}P < 0.05$, $^{**}P < 0.01$, $^{***}P < 0.001$ versus the EAE group or LPS group.

Our findings demonstrated that the Compound 21 group rats had remarkably lower EAE incidence, maximum clinical score, and mean clinical score than the EAE group rats. Besides neurological deficits, the EAE group rats exhibited more severe symptoms during the experiment, including visible lethargy, worse appetites, nasal and orbital hemorrhage, and incontinence, supporting that Compound 21 effectively attenuates EAE. Using H&E staining, we found that Compound 21 administration effectively inhibits the infiltration of immune cells in the CNS of EAE rats. In addition, EAE rats treated with Compound 21 had reduced demyelination, as revealed by LFB staining and IHC analysis. By contrast, FTY720 showed no significant difference in protecting demyelination, which is consistent with other studies [49,50]. Therefore, our study showed that Compound 21 treatment is protective against EAE in rats, and the pathological results suggest that inhibiting infiltrated immune cells contributes to this effect.

Of all the infiltrated immune cells in the CNS, Th1 and Th17 cells have been shown to be critical in the pathogenesis of MS[7]. In patients with MS, Th1 and Th17 cells, as well as the cytokines produced by them, are elevated [26,37,51]. Both the activation of Th1/Th17 cells and their subsequent infiltration into the CNS are pivotal procedures in the onset and development of MS [26,52–54]. To further explore the underlying mechanisms of Compound 21, we detected Th1/Th17 cells in EAE rats using qPCR, flow cytometry, and IHC analysis. In agreement with previous findings, our findings revealed a remarkable increase in Th1/Th17 cell numbers in both the periphery and the CNS of EAE rats. Consistent with attenuating the clinical symptoms of EAE rats, Compound 21 treatment effectively reduced the population of Th1/Th17 cells and inhibited their infiltration into the CNS. Moreover, ELISA results further confirmed the compound's suppression of the Th1/Th17 cell population. Meanwhile, Compound 21 demonstrated comparable effects on Th1 and Th17 cell infiltration to the positive control agent FTY720. To further determine if Compound 21 had direct effects on CD4$^+$ T cells, proliferation, apoptosis, and differentiation assays *in vitro* were conducted. The results showed that Compound 21 can inhibit Th1 differentiation under polarizing conditions. After being treated with Compound 21, Th0 cells still differentiated into Th17 cells, but the process was not as efficient as in the absence of Compound 21. All these findings suggest that Compound 21 treatment partially suppresses the population and infiltration of Th1/Th17 cells by directly inhibiting Th1/Th17 cell differentiation without any effects on proliferation or apoptosis.

Besides these effects, Compound 21 treatment may also inhibit Th1/Th17 cell infiltration by suppressing proinflammatory microglial cells in the CNS. Some inflammatory cytokines produced by proinflammatory microglia have shown to be significant in the activation of pathogenic Th1/Th17 cells in the CNS [39]. IL-12, IFN-γ, and TNF-α are required for Th1 cell differentiation. For Th17 cells, TGF-β, and IL-6 can promote their differentiation. IL-21 is responsible for Th17 cell amplification and IL-23 is important in stabilizing activated Th17 cells25, 27. The lack of these cytokines may contribute to the differentiation and stabilization of Th1/Th17 cells in the CNS. The findings of the co-culture experiment with BV2 cells and naïve CD4$^+$ T cells suggest that the inhibition of proinflammatory microglial cells is involved in suppressing infiltrated Th1/Th17 cell differentiation by Compound 21. To determine whether Compound 21 treatment inhibited the proinflammatory activity of microglia by reducing cytokine production, we detected the expression levels of some representative cytokines both *in vivo* and *in vitro*. The qPCR results demonstrated that the proinflammatory cytokines including *Il12a*, *Il23*, and *Il1b* declined significantly in the spinal cord and the brain of EAE rats after Compound 21 treatment. The experiment *in vitro* showed that the expression of these related cytokines were elevated in LPS-induced microglial cells and remarkably reduced by Compound 21 treatment. These results further indicate that suppression of the proinflammatory microglia is an underlying mechanism of Compound 21 to downregulate Th1/Th17 infiltration in EAE rats.

Local microglial cells can be activated into two phenotypes: the proinflammatory M1 phenotype, which promotes EAE pathogenesis; and the anti-inflammatory M2 phenotype, which attenuates the disease [38,39]. In this study, we further detected the M1/M2 polarization of microglial cells both *in vivo* and *in vitro*. The results illustrated that EAE rats possess a high proportion of proinflammatory microglia in the CNS; Compound 21 administration significantly suppressed the stimulation of M1 microglial cells and increased the percentage of M2 microglial cells both *in vivo* and *in vitro*. We suggest that the anti-inflammatory effect of Compound 21 administration is related to the regulation of M1/M2 polarization. Collectively, Compound 21 treatment switched the polarization of microglial cells to reduce the generation of inflammatory cytokines, thus affecting the infiltrated Th1/Th17 cell differentiation and stabilization in the CNS. However, further mechanisms still need to be elucidated to determine how Compound 21 treatment regulates the activation of microglia and which pathways are altered in the suppression of Th1/Th17 cell differentiation.

All the protective effects of Compound 21 on EAE rats suggest its role as a novel candidate for MS treatment. However, several potential challenges exist in developing Compound 21 for clinical use. First, it is far from clear whether this compound exerts similar effects in humans, so further *in vivo* studies and clinical trials are needed. Second, the pharmacokinetic and pharmacodynamic features of Compound 21 in humans may differ from those in animals and need more specific evaluation. Lastly, although no side effects of Compound 21 have been detected in animal models, its side effects should be carefully evaluated for clinical use. Because Compound 21 exerts inhibitory effects on inflammation and immune response, possible effects related to immune suppression should be carefully examined.

5. Conclusions

Taken together, we report for the first time that the novel phloroglucinol derivative Compound 21 can attenuate neurological deficits and demyelination in the EAE rat model by decreasing the population and infiltration of Th1/Th17 cells. This protective effect is probably mediated by directly suppressing Th1/Th17 cell differentiation and inhibiting the activation of proinflammatory microglial cells in the CNS. The current investigation provides evidence that Compound 21 may be a novel candidate for MS treatment.

Uncited references

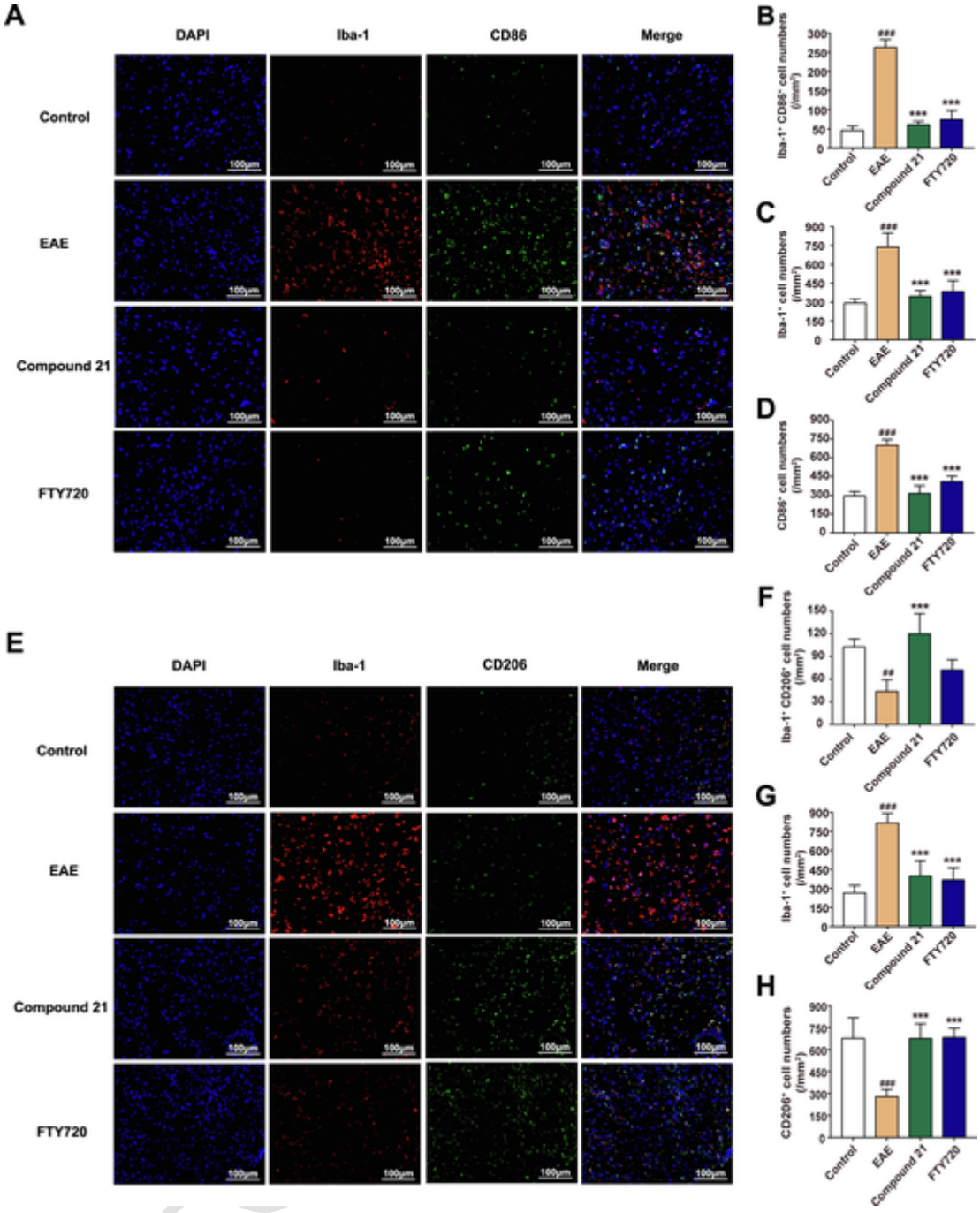

Fig. 6. Compound 21 treatment reduced M1 phenotype of microglial cells and increased M2 phenotype of microglial cells *in vivo*. (A) Representative captures of immunofluorescence in the corpus callosum region of nuclei (DAPI, blue), total microglial cells (Iba-1, red), and M1 phenotype microglial cells (CD86, green). (B) The numbers of Iba-1$^+$/CD86$^+$ cells. (C) The numbers of Iba-1$^+$ cells. (D) The numbers of CD86$^+$ cells. (E) Representative captures of immunofluorescence in the corpus callosum region of nuclei (DAPI, blue), total microglial cells (Iba-1, red) and M2 phenotype microglial cells (CD206, green). (F) The numbers of Iba-1$^+$/CD206$^+$ cells, (G) Iba-1$^+$ cells, and (H) CD206$^+$ cells. All the brain tissues were collected on day 16 post-immunization. Values are presented as the mean ± SD; n = 3 per group (3 sections per rat). $^{###}$P < 0.001 versus the Control group; ***P < 0.001 versus the EAE group.

[16–19].

Acknowledgements

This work was supported by the National Natural Sciences Foundation of China (81630097 and 81773718), the Chinese Academy of Medical Sciences Innovation Fund for Medical Sciences (2016-I2M-3-011), the Chinese Academy of Medical Sciences Fundamental Research Funds for the Central Universities (2018RC350002), and the Drug Innovation Major Project (2018ZX09711001-003-005, 2018ZX09711001-008-005, and 2018ZX09711001-003-020).

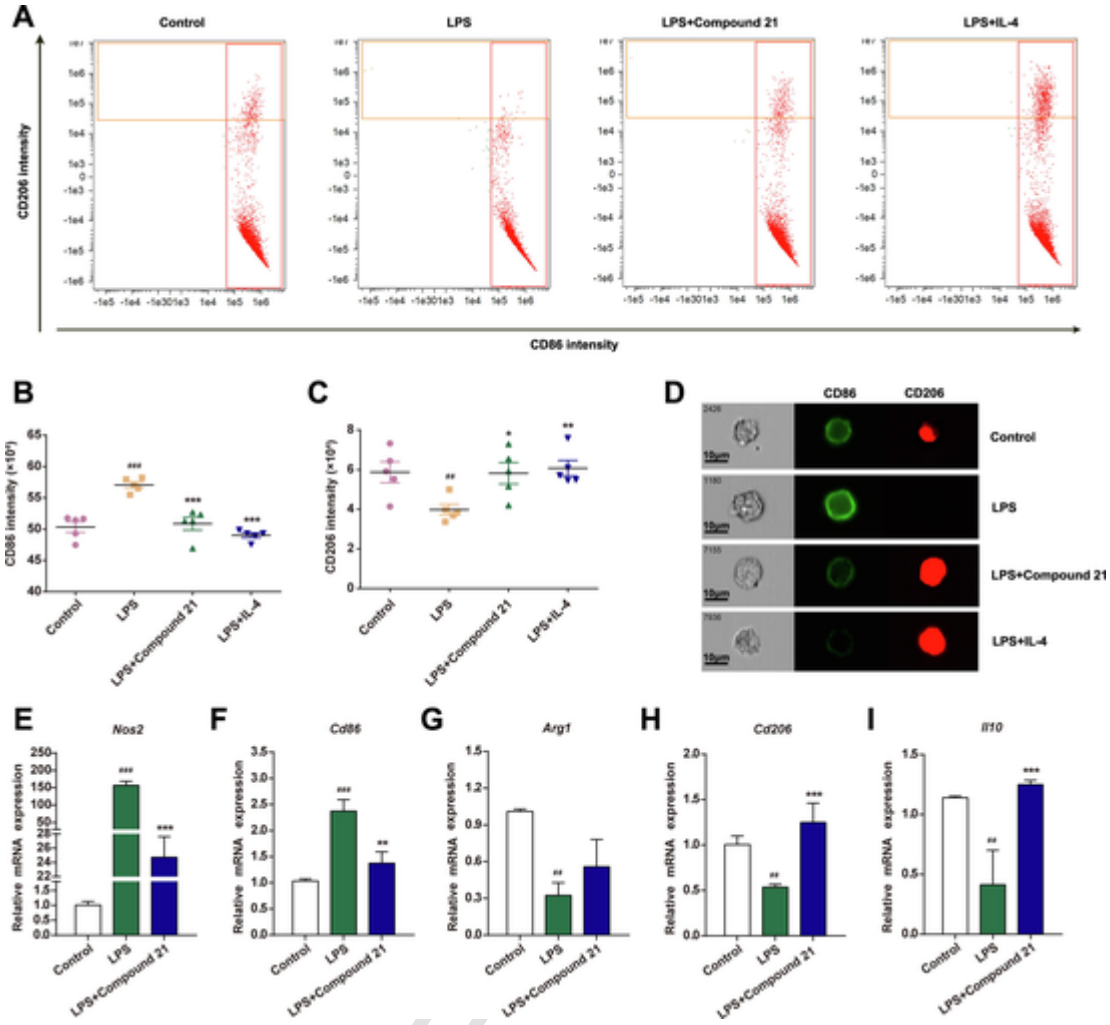

Fig. 7. Compound 21 treatment switched M1/M2 phenotypes of microglial cells *in vitro*. (A) Flow cytometric analysis of the M1 marker (CD86) and M2 marker (CD206) of BV2 cells. (B) Mean intensities of CD86 detected by flow cytometry. (C) Mean intensities of CD206 detected by flow cytometry. (D) Representative images of BV2 cells stained by CD86 and CD206. mRNA expression levels in BV2 cells: (E) *Nos2* expression, (F) *Cd86* expression, (G) *Arg1* expression, (H) *Cd206* expression, and (I) *Il10* expression. LPS, lipopolysaccharides. Values are shown as the mean ± SD; n = 5 per group for flow cytometry; n = 3 for qPCR. $^{\#\#}P < 0.01$, $^{\#\#\#}P < 0.001$ versus control cells; $^{*}P < 0.05$, $^{**}P < 0.01$, $^{***}P < 0.001$ versus LPS cells.

References

[1] D Ontaneda, A J Thompson, R J Fox, J A Cohen, Progressive multiple sclerosis: prospects for disease therapy, repair, and restoration of function, Lancet 389 (2017) 1357–1366.

[2] A H Beecham, N A Patsopoulos, D K Xifara, M F Davis, A Kemppinen, C Cotsapas, et al., Analysis of immune-related loci identifies 48 new susceptibility variants for multiple sclerosis, Nat. Genet. 45 (2013) 1353–1360.

[3] S Sawcer, R J Franklin, M Ban, Multiple sclerosis genetics, Lancet Neurol. 13 (2014) 700–709.

[4] A Ascherio, K L Munger, R White, K Kochert, K C Simon, C H Polman, et al., Vitamin d as an early predictor of multiple sclerosis activity and progression, JAMA Neurol. 71 (2014) 306–314.

[5] R A Marrie, Environmental risk factors in multiple sclerosis aetiology, Lancet Neurol. 3 (2004) 709–718.

[6] R Ramanujam, A K Hedstrom, A Manouchehrinia, L Alfredsson, T Olsson, M Bottai, et al., Effect of smoking cessation on multiple sclerosis prognosis, JAMA Neurol. 72 (2015) 1117–1123.

[7] B Hemmer, M Kerschensteiner, T Korn, Role of the innate and adaptive immune responses in the course of multiple sclerosis, Lancet Neurol. 14 (2015) 406–419.

[8] R Hohlfeld, K Dornmair, E Meinl, H Wekerle, The search for the target antigens of multiple sclerosis, part 1: Autoreactive cd4+ t lymphocytes as pathogenic effectors and therapeutic targets, Lancet Neurol. 15 (2016) 198–209.

[9] L Schirmer, R Srivastava, B Hemmer, To look for a needle in a haystack: the search for autoantibodies in multiple sclerosis, Mult. Scler. 20 (2014) 271–279.

[10] M Kipp, S Nyamoya, T Hochstrasser, S Amor, Multiple sclerosis animal models: a clinical and histopathological perspective, Brain Pathol. 27 (2017) 123–137.

[11] R M Ransohoff, Animal models of multiple sclerosis: the good, the bad and the bottom line, Nat. Neurosci. 15 (2012) 1074–1077.

[12] A J Thompson, S E Baranzini, J Geurts, B Hemmer, O Ciccarelli, Multiple sclerosis, Lancet 391 (2018) 1622–1636.

[13] P A Calabresi, B C Kieseier, D L Arnold, L J Balcer, A Boyko, J Pelletier, et al., Pegylated interferon beta-1a for relapsing-remitting multiple sclerosis (advance): a randomised, phase 3, double-blind study, Lancet Neurol. 13 (2014) 657–665.

[14] E Le Page, D Veillard, D A Laplaud, S Hamonic, R Wardi, C Lebrun, et al., Oral versus intravenous high-dose methylprednisolone for treatment of relapses in patients with multiple sclerosis (copousep): a randomised, controlled, double-blind, non-inferiority trial, Lancet 386 (2015) 974–981.

[15] Efficacy and toxicity of cyclosporine in chronic progressive multiple sclerosis: A randomized, double-blinded, placebo-controlled clinical trial. The multiple sclerosis study group. Ann. Neurol. 1990, 27, 591–605.

[16] T Chitnis, D L Arnold, B Banwell, W Bruck, A Ghezzi, G Giovannoni, et al., Trial of fingolimod versus interferon beta-1a in pediatric multiple sclerosis, N. Engl. J. Med. 379 (2018) 1017–1027.

[17] P A Calabresi, E W Radue, D Goodin, D Jeffery, K W Rammohan, A T Reder, et al., Safety and efficacy of fingolimod in patients with relapsing-remitting multiple sclerosis (freedoms ii): a double-

blind, randomised, placebo-controlled, phase 3 trial, Lancet Neurol. 13 (2014) 545–556.
[18] F Lublin, D H Miller, M S Freedman, B A C Cree, J S Wolinsky, H Weiner, et al., Oral fingolimod in primary progressive multiple sclerosis (informs): a phase 3, randomised, double-blind, placebo-controlled trial, Lancet 387 (2016) 1075–1084.
[19] J P DiMarco, P O'Connor, J A Cohen, A T Reder, L Zhang-Auberson, D Tang, et al., First-dose effects of fingolimod: pooled safety data from three phase 3 studies, Mult. Scler. Relat. Disord. 3 (2014) 629–638.
[20] M Clerico, C A Artusi, A D Liberto, S Rolla, V Bardina, P Barbero, et al., Natalizumab in multiple sclerosis: Long-term management, Int. J. Mol. Sci. 18 (2017) 940.
[21] T Kalincik, J W L Brown, N Robertson, M Willis, N Scolding, C M Rice, et al., Treatment effectiveness of alemtuzumab compared with natalizumab, fingolimod, and interferon beta in relapsing-remitting multiple sclerosis: a cohort study, Lancet Neurol. 16 (2017) 271–281.
[22] V Brucklacher-Waldert, K Stuerner, M Kolster, J Wolthausen, E Tolosa, Phenotypical and functional characterization of t helper 17 cells in multiple sclerosis, Brain 132 (2009) 3329–3341.
[23] I Kleiter, J Song, D Lukas, M Hasan, B Neumann, A L Croxford, et al., Smad7 in t cells drives t helper 1 responses in multiple sclerosis and experimental autoimmune encephalomyelitis, Brain 133 (2010) 1067–1081.
[24] H Lassmann, R M Ransohoff, The cd4-th1 model for multiple sclerosis: A critical correction of crucial] re-appraisal, Trends Immunol. 25 (2004) 132–137.
[25] D D Patel, V K Kuchroo, Th17 cell pathway in human immunity: Lessons from genetics and therapeutic interventions, Immunity 43 (2015) 1040–1051.
[26] C A Dendrou, L Fugger, M A Friese, Immunopathology of multiple sclerosis, Nat. Rev. Immunol. 15 (2015) 545–558.
[27] J Zepp, L Wu, X Li, Il-17 receptor signaling and t helper 17-mediated autoimmune demyelinating disease, Trends Immunol. 32 (2011) 232–239.
[28] U K Hanisch, H Kettenmann, Microglia: active sensor and versatile effector cells in the normal and pathologic brain, Nat. Neurosci. 10 (2007) 1387–1394.
[29] Y Tang, W Le, Differential roles of m1 and m2 microglia in neurodegenerative diseases, Mol. Neurobiol. 53 (2016) 1181–1194.
[30] Y D Wang, X Q Bao, S Xu, W W Yu, S N Cao, J P Hu, et al., A novel parkinson's disease drug candidate with potent anti-neuroinflammatory effects through the src signaling pathway, J. Med. Chem. 59 (2016) 9062–9079.
[31] C Zang, H Yang, L Wang, Y Wang, X Bao, X Wang, et al., A novel synthetic derivative of phloroglucinol inhibits neuroinflammatory responses through attenuating kalirin signaling pathway in murine bv2 microglial cells, Mol. Neurobiol. 56 (2018) 2870–2880.
[32] Z Zhao, X Q Bao, Z Zhang, H Liu, D Zhang, Phloroglucinol derivative compound 21 attenuates cuprizone-induced multiple sclerosis mice through promoting remyelination and inhibiting neuroinflammation, Sci. China Life Sci. (2019), doi:10.1007/s11427-019-9821-2.
[33] L Kremer, O Taleb, N Boehm, A G Mensah-Nyagan, E Trifilieff, J de Seze, et al., Fty720 controls disease severity and attenuates sciatic nerve damage in chronic experimental autoimmune neuritis, J. Neuroinflammat. 16 (2019) 54.
[34] H Kataoka, K Sugahara, K Shimano, K Teshima, M Koyama, A Fukunari, et al., Fty720, sphingosine 1-phosphate receptor modulator, ameliorates experimental autoimmune encephalomyelitis by inhibition of t cell infiltration, Cell Mol. Immunol. 2 (2005) 439–448.
[35] E Beraud, A Viola, I Regaya, S Confort-Gouny, P Siaud, D Ibarrola, et al., Block of neural kv1.1 potassium channels for neuroinflammatory disease therapy, Ann. Neurol. 60 (2006) 586–596.
[36] M J Lee, M Jang, J Choi, G Lee, H J Min, W S Chung, et al., Bee venom acupuncture alleviates experimental autoimmune encephalomyelitis by upregulating regulatory t cells and suppressing th1 and th17 responses, Mol. Neurobiol. 53 (2016) 1419–1445.
[37] G Arellano, E Acuna, L I Reyes, P A Ottum, P De Sarno, L Villarroel, et al., Th1 and th17 cells and associated cytokines discriminate among clinically isolated syndrome and multiple sclerosis phenotypes, Front. Immunol. 8 (2017) 753.
[38] J F Bogie, P Stinissen, J J Hendriks, Macrophage subsets and microglia in multiple sclerosis, Acta Neuropathol. 128 (2014) 191–213.
[39] S Voet, M Prinz, G van Loo, Microglia in central nervous system inflammation and multiple sclerosis pathology, Trends Mol. Med. 25 (2019) 112–123.
[40] V E Miron, A Boyd, J W Zhao, T J Yuen, J M Ruckh, J L Shadrach, et al., M2 microglia and macrophages drive oligodendrocyte differentiation during cns remyelination, Nat. Neurosci. 16 (2013) 1211–1218.
[41] I Francos-Quijorna, J Amo-Aparicio, A Martinez-Muriana, R Lopez-Vales, Il-4 drives microglia and macrophages toward a phenotype conducive for tissue repair and functional recovery after spinal cord injury, Glia 64 (2016) 2079–2092.
[42] X Zhao, H Wang, G Sun, J Zhang, N J Edwards, J Aronowski, Neuronal interleukin-4 as a modulator of microglial pathways and ischemic brain damage, J. Neurosci. 35 (2015) 11281–11291.
[43] R Gold, C Linington, H Lassmann, Understanding pathogenesis and therapy of multiple sclerosis via animal models: 70 years of merits and culprits in experimental autoimmune encephalomyelitis research, Brain 129 (2006) 1953–1971.
[44] C S Constantinescu, N Farooqi, K O'Brien, B Gran, Experimental autoimmune encephalomyelitis (eae) as a model for multiple sclerosis (ms), Br. J. Pharmacol. 164 (2011) 1079–1106.
[45] V Brinkmann, A Billich, T Baumruker, P Heining, R Schmouder, G Francis, et al., Fingolimod (fty720): discovery and development of an oral drug to treat multiple sclerosis, Nat. Rev. Drug Discov. 9 (2010) 883–897.
[46] A Eken, M F Yetkin, A Vural, F Z Okus, S Erdem, Z B Azizoglu, et al., Fingolimod alters tissue distribution and cytokine production of human and murine innate lymphoid cells, Front. Immunol. 10 (2019) 217.
[47] S Mandala, R Hajdu, J Bergstrom, E Quackenbush, J Xie, J Milligan, et al., Alteration of lymphocyte trafficking by sphingosine-1-phosphate receptor agonists, Science 296 (2002) 346–349.
[48] M Matloubian, C G Lo, G Cinamon, M J Lesneski, Y Xu, V Brinkmann, et al., Lymphocyte egress from thymus and peripheral lymphoid organs is dependent on s1p receptor 1, Nature 427 (2004) 355–360.
[49] Y Zhang, X Li, B Ciric, C G Ma, B Gran, A Rostami, et al., Effect of fingolimod on neural stem cells: a novel mechanism and broadened application for neural repair, Mol. Ther. 25 (2017) 401–415.
[50] A Slowik, T Schmidt, C Beyer, S Amor, T Clarner, M Kipp, The sphingosine 1-phosphate receptor agonist fty720 is neuroprotective after cuprizone-induced cns demyelination, Br. J. Pharmacol. 172 (2015) 80–92.
[51] S Hagman, M Raunio, M Rossi, P Dastidar, I Elovaara, Disease-associated inflammatory biomarker profiles in blood in different subtypes of multiple sclerosis: prospective clinical and mri follow-up study, J. Neuroimmunol. 234 (2011) 141–147.
[52] H L Weiner, A shift from adaptive to innate immunity: a potential mechanism of disease progression in multiple sclerosis, J. Neurol. 255 (Suppl 1) (2008) 3–11.
[53] R M Ransohoff, B Engelhardt, The anatomical and cellular basis of immune surveillance in the central nervous system, Nat. Rev. Immunol. 12 (2012) 623–635.
[54] J Correale, M I Gaitan, M C Ysrraelit, M P Fiol, Progressive multiple sclerosis: From pathogenic mechanisms to treatment, Brain 140 (2017) 527–546.